Journal of Materials Science: Materials in Electronics (2018) 29:15931–15945
https://doi.org/10.1007/s10854-018-9679-7

Enhancement of dielectric properties and AC electrical conductivity of nanocomposite using poly (vinyl chloride-co-vinyl acetate-co-2-hydroxypropyl acrylate) filled with graphene oxide

A. Y. Yassin[1,2] · A. Raouf Mohamed[2] · A. M. Abdelghany[3] · E. M. Abdelrazek[4]

Received: 6 April 2018 / Accepted: 16 July 2018 / Published online: 19 July 2018

Abstract
Synthesis of a new nanocomposite composed of poly (vinyl chloride-co-vinyl acetate-co-2-hydroxypropyl acrylate) (PVVH) copolymer and graphene oxide (GO) was successfully achieved using solution casting technique. Dielectric properties of the nanocomposite were investigated in the frequency range (10 Hz to 10 MHz) over the temperature range (298–373 K). Many variables such as: dielectric constant, dielectric loss, loss tangent, electric moduli and AC conductivity were studied with changing frequency and temperature, showing improvement in the nanocomposite properties with both of them. The non-Debye behaviour of the samples was confirmed from the electric modulus analysis. AC conductivity (σ_{ac}) was found to follow Jonscher's universal power law. The enhancement in (σ_{ac}) with frequency and temperature has implied the presence of free charge carriers that pass by hopping through defect sites over the potential barriers separating them in the PVVH/GO matrix. The correlated barrier hopping (CBH) model was found to be the best choice for describing AC conduction mechanism in the current nanocomposite over the above temperature range. Scaling of (σ_{ac}) carried out for the prepared samples has exhibited that charge carriers within the current matrix follow a common conduction mechanism. A comparison between maximum barrier height and activation energy has been carried out to demonstrate the charge carriers transport mechanism. The PVVH-based nanocomposite with the highest concentration of GO (4 wt%) has achieved the highest enhancement in (σ_{ac}) and mechanical properties, suggesting the feasibility of using it in designing electrochemical and energy storage devices.

1 Introduction

Nowadays, nanoscience and nanotechnology play an efficient and essential role in our daily lives which are largely affected by the development introduced into materials, especially in the nanometer range. These novel materials with improved functionality are significantly useful in numerous fields such as; medical, biological, material science, as well as engineering fields, extending to industrial and electronic applications, etc. One of those substantial improved properties is the dielectric properties which pave the way for introducing many significant applications such as; sensors, microwave devices, high storage devices, electrical and electronic industries [1–5].

Carbon-based materials such as; carbon nanotube, black carbon, graphene and graphene-related materials (including graphene oxide) are widely used as nanofillers for improving the dielectric properties of the polymers owing to their large surface area, which endow nanocomposites prepared with a good interfacial polarization [3, 6]. One of these promising nanofillers is graphene oxide (GO), which is defined as a 2D conductive material composed of monolayer of graphite oxide and represents the contiguous arrangement of sp^2 carbon–carbon bonds packed densely in hexagonal shape to form a honeycomb lattice based on the hybridized carbon atoms. It is also characterized by a few oxygen-containing groups on its basal plane and edges [7, 8].

It is worth mentioning that GO is much better in forming nanocomposites with good mechanical and dielectric

✉ A. Y. Yassin
a_yassin2200@yahoo.com

1 Dental Biomaterial Department, Faculty of Oral & Dental Medicine, Delta University for Science & Technology, Gamassa, Egypt

2 Physics Department, Faculty of Science, Port-Said University, Port-Said, Egypt

3 Spectroscopy Department, Physics Division, National Research Center, Cairo, Egypt

4 Physics Department, Faculty of Science, Mansoura University, Mansoura, Egypt

properties than other traditional dielectric fillers. The reason is because it successfully create percolation structure with only small quantity in order to keep up these properties without breaking down for potential applications related to energy storage and high performance electromagnetic shielding. Moreover, its oxygen-containing functional groups such as; hydroxyl, carboxyl, carbonyl and epoxide groups could considerably useful for enhancing the interfacial interaction of GO with polymers used [9], forming hydrogen bonds and consequently strengthen the nanocomposites obtained. In addition to increment in interfaces leads to increasing the interfacial polarization which means improving dielectric properties of the polymer nanocomposites.

Polarization of polymer nanocomposites in an electric field is another side that represents dielectric constant, so that the enhancement in one of them implies improving the other one and vice versa.

Generally, dielectric constant for most polymers are very weak, so researchers [4, 10–14] over the last few decades have tried to overcome this problem by incorporating (one or more) fillers into polymers matrices. Several methods have been carried out in an attempt to produce and develop more efficient dielectrics characterized by high dielectric constant as well as low dielectric loss, which are highly desirable [15, 16]. The significant expansion in scientific interest with polymer nanocomposites has stemmed from their low cost, high compression strength, easy processability and their ability to improve numerous properties of advanced materials to meet the necessity [17, 18].

Poly (vinyl chloride-co-vinyl acetate-co-2-hydroxypropyl acrylate) (PVVH) is a copolymer composed of 81 wt% vinyl chloride, 15 wt% 2-hydroxypropyl acrylate and 4 wt% vinyl acetate monomers. It is transparent, sensitive to changes in temperature and flexible copolymer with good film formation property.

Only few reports for PVVH have been found in literature [19–23]. Ahmed et al. [21–23] reported the dielectric properties of PVVH using TSDC-TS technique. Whereas some polymer composites with GO were reported in order to improve flexibility, structural, thermal, electrical, mechanical and dielectric properties [17, 23–27]. Tantis et al. [12] have fabricated nanocomposites based on PVA and chemically derivatized graphene via combining solution processing and compression molding. In their study, dielectric measurements exhibited enhancement of the electrical permittivity for the prepared nanocomposites. Despite all these researches, further modifications on polymers are still required to improve their dielectric properties to meet the necessity for fabricating high energy storage devices with high performance and low cost.

In the present study, GO has been synthesized in a simple approach from natural graphite by modified Hammers method. PVVH/GO nanocomposites have been mainly prepared by varying GO concentration using a solution casting process to improve their dielectric and mechanical properties. This work has been also carried to investigate their AC conductivity for using them in potential applications such as; high energy storage devices and embedded capacitors. Comparison between maximum barrier height and activation energy has been performed with a view to gain an insight into the charge carriers transport mechanism. More details are mentioned in the following sections.

2 Experimental details

2.1 Materials

All chemicals used were purchased from Sigma-Aldrich and are of analytical reagent grade. PVVH of (81 wt% vinyl chloride; 15 wt% 2-hydroxypropyl acrylate; 4 wt% vinyl acetate) has molecular weight *ca*. 33,000 g/mol. Potassium permanganate ($KMnO_4$) and sulphuric acid (H_2SO_4) were used as oxidant agents. Natural graphite nanopowder was bought for preparing graphene oxide by modified Hammers method [28]. Tetrahydrofuran (THF) was purchased from Fisher Scientific (UK) for dissolving PVVH.

2.2 Preparation of graphene oxide

The preparation steps are shown in Fig. 1. In brief, 3 g of graphite powder and 150 mL conc. sulphuric acid were mixed together with stirring the solution mixture in ice bath for 1.5 h. Then, 11 g of $KMnO_4$ was carefully added in small amounts with increasing temperature to 40 °C for 40 min. After 12 h, 250 mL of distilled water was gradually added with heating the mixture to 98 °C for 30–40 min, then followed by adding 10 mL of hydrogen peroxide (30%). The resultant collected product was washed several times with aqueous solution of HCl and distilled water. The final product was dried at 55 °C in oven for 24 h.

2.3 PVVH/GO nanocomposite preparation

PVVH (3.5 g) dissolved in 350 mL of THF was mixed together with GO solution with stirring the mixture for 3 h at 40 °C. GO was added with different concentrations (0.2, 0.4, 0.8, 1.6, 3 and 4 wt%; symbolized as PG1, PG2, PG3, PG4, PG5, PG6), then were sonicated for 30 min. Pure PVVH film designated as PG0 was prepared under the same conditions to use as a reference. Finally, the mixtures resulted were carefully dropped onto clean glass Petri dishes, and then were left to dry for 48 h at room temperature.

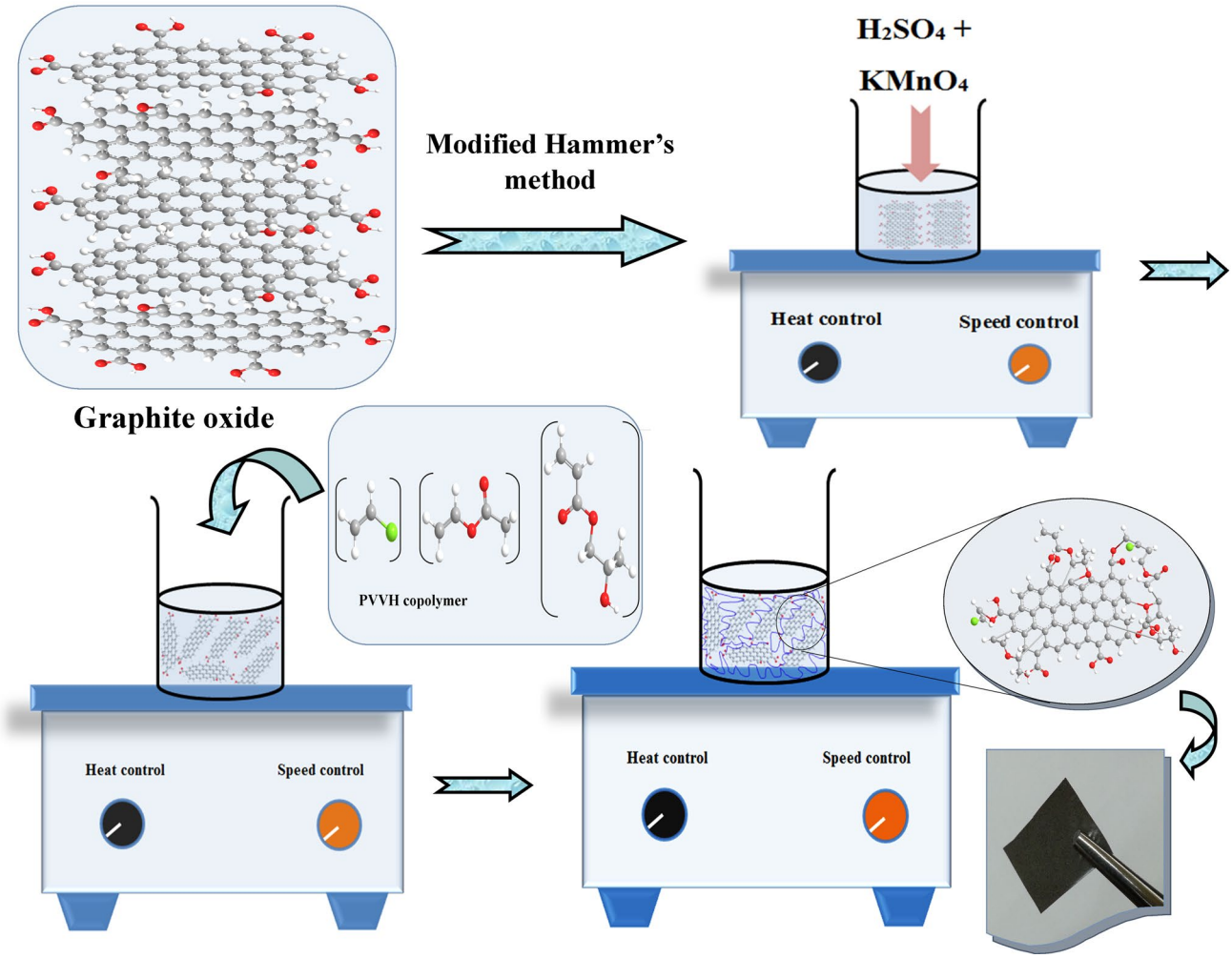

Fig. 1 Preparation steps of PVVH/GO nanocomposites

2.4 Measurements

XRD analysis for GO was carried out using DIANO corporation, USA with Cu-Kα radiation (λ = 1.5406 Å) at 15 kV in the range of 2θ = 5°–60° at room temperature. Moreover, pure GO resulted was characterized using Nicolet *iS*10 type FT-IR spectrometer, USA in the range of 4000–400 cm^{-1}, while its Raman spectrum was recorded via Raman spectrometer (LABRAM HR) equipped with 633 nm laser. The dielectric properties of the prepared samples and their AC conductivity were carried out using the broadband dielectric spectrometer with Novo control technology in combination with QUATRO Cryo-system (concept 40), which has temperature stability ± 0.01 °C. The results were recorded in the frequency range from 10 Hz to 10 MHz with changing temperature from room temperature to 373 K. Mechanical properties were examined using LS universal testing machine from Lloyd Instruments (UK) with high accuracy YLC series load cells.

3 Results and discussion

3.1 Characterization of GO

In order to study the degree of exfoliation and confirm the successful synthesis of GO from natural graphite, X-ray diffraction technique was used and the corresponding pattern is shown in Fig. 2. The peak observed at 2θ ≈ 10.5° is attributed to GO, and corresponds to (001) diffraction plane [15, 29]. Absence of the characteristic peak of graphite at 2θ ≈ 26° implies that GO sheets were efficiently exfoliated into individual sheets.

Further, the synthesized GO was investigated by FT-IR and Raman spectroscopy to provide a deeper insight into its chemical structure for completing the picture. Figure 3 exhibits FT-IR spectrum of GO in the region 4000–400 cm^{-1}, where its characteristic peaks were observed. The broad peak at 3420 cm^{-1} is ascribed to O–H stretching vibration that originated from hydroxyl groups

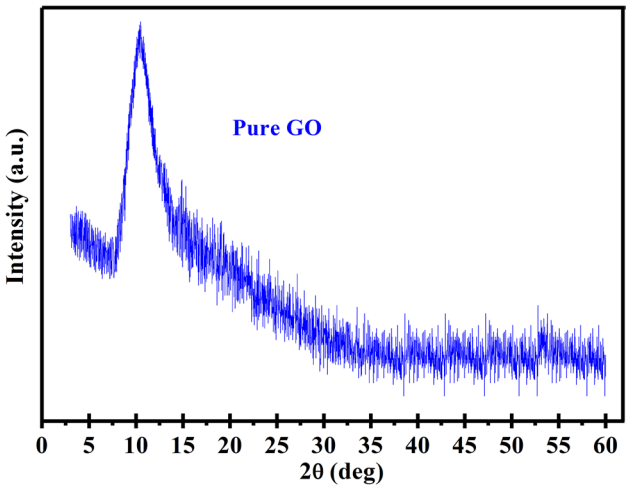

Fig. 2 XRD pattern of pure graphene oxide

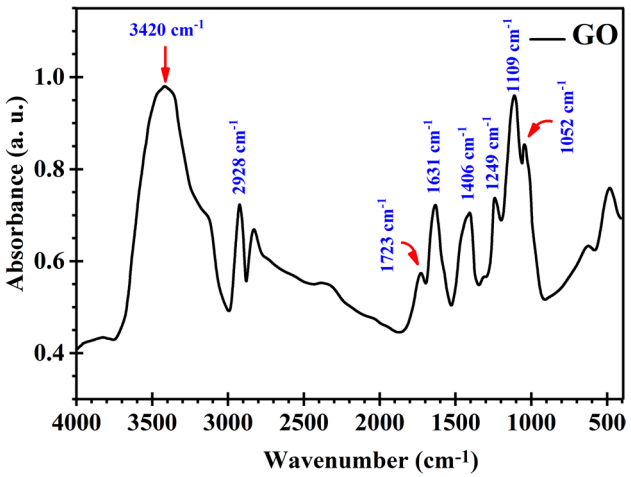

Fig. 3 FT-IR spectrum of GO in the region 4000–400 cm^{-1}

on the basal plane of GO. The distinct bands at 2928, 1723 and 1623 cm^{-1} are attributed to asymmetric CH_2 stretching, C=O stretching of COOH functional groups and C=C skeletal vibration, respectively [11, 24]. The bands that represent C−O stretching vibrations of carboxyl, epoxide and alkoxy groups of GO are detected at 1406, 1249 and 1052 cm^{-1}, respectively [30].

Furthermore, the Raman spectrum of GO is depicted in Fig. 4, which consists of two characteristic bands. The intense peak at 1350 cm^{-1} is attributed to D band, which corresponds to SP^3 hybridized carbon, implying the presence of defects and disordered carbon. The broad band observed at 1590 cm^{-1} is ascribed to G band related to the vibration of ordered SP^2 hybridized carbon [25, 29]. The intensity ratio of D band to G band (I_D/I_G) is 0.83, which is in agreement with the results reported by Frindy et al. [31] and Deshmukh et al. [24]. This result indicates that many defects are created

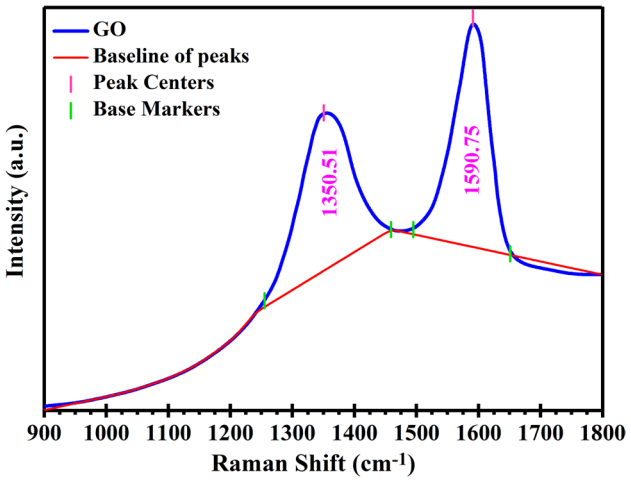

Fig. 4 Raman spectrum of GO

and a high level of disorder in GO layers are introduced through oxidation and ultrasonic exfoliation of graphite, confirming the successful synthesis of GO.

3.2 Dielectric spectra analysis

3.2.1 Variation of dielectric constant and dielectric loss with frequency and temperature

Complex permittivity is generally employed for providing a successful description about dielectric behaviour of a material, and is given by [32]:

$$\varepsilon^* = \varepsilon' - i\varepsilon'' \tag{1}$$

where, ε′ is the dielectric constant that represents the stored energy and ε" is the dielectric loss which represents the dissipated energy. Real and imaginary parts of the dielectric constant (ε′) and (ε″), respectively are calculated using the following relations [11]:

$$\varepsilon' = \frac{C_p}{\varepsilon_o}\frac{d}{A} \tag{2}$$

$$\varepsilon'' = \frac{\sigma}{\omega\varepsilon_o} \tag{3}$$

where C_p is the capacitance of the sample under investigation measured in parallel mode, d its thickness, A is the electrode cross-sectional area, ω is the angular frequency and ε_o ($=8.85\times10^{-12}$ F/m) is the permittivity of free space.

Figure 5a shows the frequency dependence of (ε′) of PG0 at various temperatures. From the graphs, it is evident that ε′ at low frequencies has attained higher values and have been increased with temperature. PVVH copolymer is characterized by the presence of vinyl chloride, vinyl acetate and

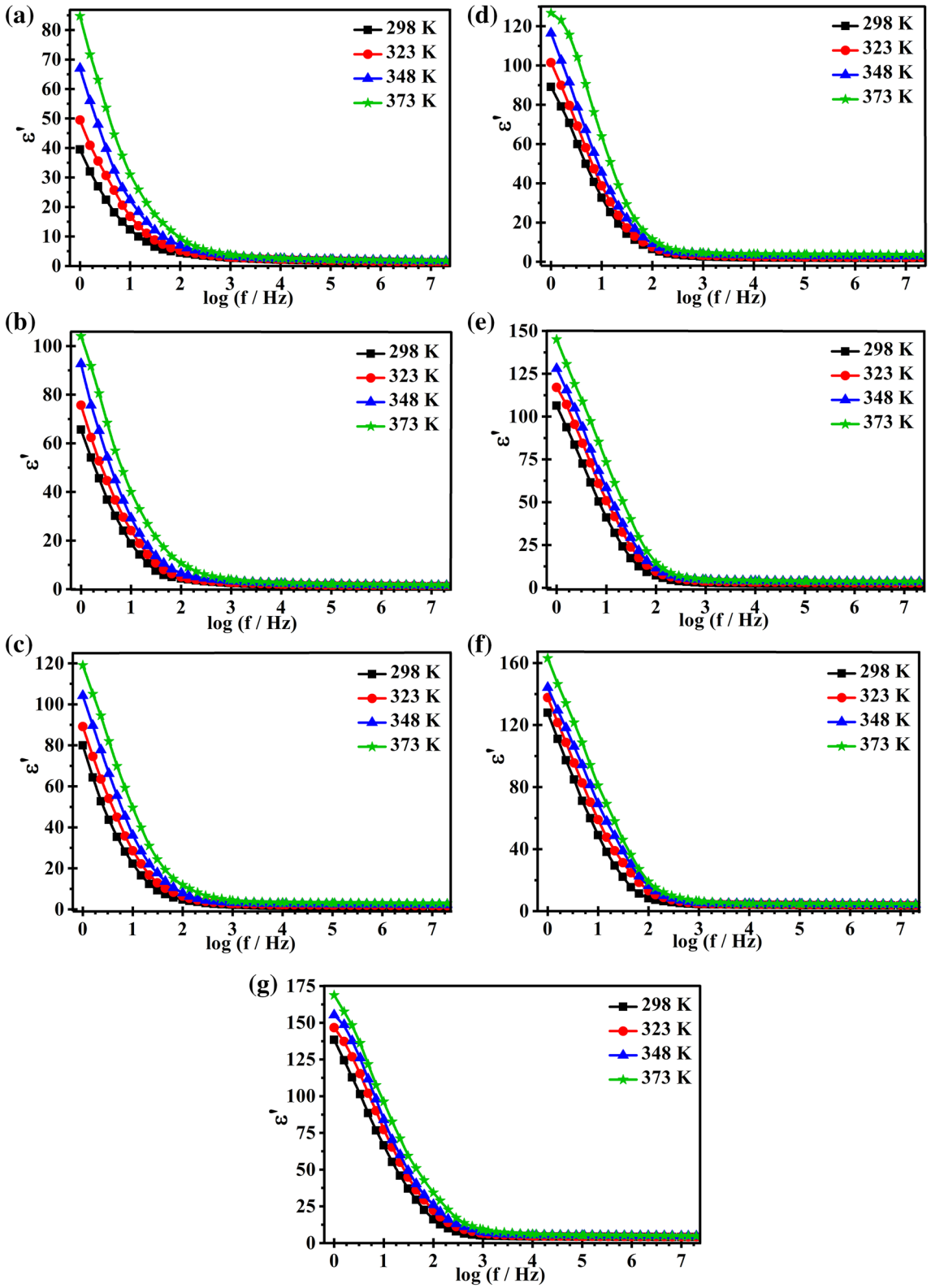

Fig. 5 The frequency dependence of (ε′) of **a** PG0, **b** PG1, **c** PG2, **d** PG3, **e** PG4, **f** PG5, **g** PG6 at various temperatures

2-hydroxypropyl acrylate monomers. These monomers contain polar functional groups such as –OH, C=O, ≡CCl, HCl, etc., where dipoles are created because of the imbalance in electrons distribution. These dipoles orient themselves with the electric field, increasing dipole polarization. Also, they have a receptivity to absorb moisture from the atmosphere, where the presence of moisture increases the dielectric constant and reduces resistivity. With the increase in temperature, polymer chains move faster as well as dipoles follow the rapid and periodic alternation of the field direction, raising the dielectric constant values. Moreover, this may be attributed to the dominance of electrode polarization, where space charges exist at the interfaces between PG0 sample and the electrode.

Figure 5b-g shows the frequency dependence of (ε′) of PVVH filled with different levels of GO at various temperatures. From the graphs, it is evident that ε′ at low frequencies has attained higher values and have been enhanced with increasing temperature, denoting the dominance of electrode polarization, and this confirms the non-Debye behavior of the samples [33]. While at high frequencies, it has decreased rapidly and became relatively constant with the change in frequency. The high values of ε′ at low frequencies are due to accumulation of unbounded charge carriers at the interfaces of PVVH with GO, where they do not have enough energy to overcome the potential barrier that restricts them [12, 34]. Further, in the low-frequency region—the permanent and induced dipoles had enough time to easily follow the slow alternation of the applied field by aligning themselves to be in the same direction, thereby enhancing polarization. On the other hand, the (ε′) value in the high-frequency region shows a slight change with increasing frequency, because it has resulted only from the small contributions of ionic and electronic polarization.

In other words, the decrease in (ε′) observed at higher frequencies has resulted from the inability of charge carriers to follow the rapid and periodic alternation of the field direction, as well as it has originated from the decrease in interfacial polarization that took place owing to the accumulation of charges at the PVVH–GO interfaces [35].

The high values of (ε′), i.e., stored energy, especially at low frequencies, are assigned to either improved conductivity, interfacial polarization, electrode polarization or all of them. Electrode polarization (EP) is due to the existence of space charges at the interfaces between the electrode and the sample under investigation and it is distinguished by very high values of both (ε′) and (ε″) [35, 36]. All samples were investigated under the same conditions and had similar constituents. Therefore, if EP had the greatest effect in a certain sample, it would be the dominant in all other samples as well. Taking this point of view into account, the high value of (ε′) is assigned to conductivity and interfacial polarization. The sample with the highest concentration of GO (PG6) has achieved the best electrical enhancement, which recommends using this nanocomposite in designing energy storage devices.

In the literature, the same behavior of increasing dielectric constant with the increase in the filler content has reported in some studies [24, 37]. This increase is assigned to the formation of microcapacitors within PVVH matrix due to the presence of conducting GO.

The variation of (ε″) with frequency for the PVVH/GO nanocomposites is represented in Fig. 6a–g. The distinct increase in (ε″) when incorporating GO into the PVVH matrix, is due to the electrical conductive nature of GO. The temperature dependence of (ε′) and (ε″) for the current system displayed in Figs. 5 and 6 are due to the high charge carriers' density as well as the increase in DC contribution. ε″ largely depends on temperature; because the higher the temperature, the greater the degree of dissociation and re-dissociation of ions aggregations, consequently increasing the free charge carriers' density [35]. Few of these charge carriers may leak by creating tunneling path causing the observed increase in dissipated energy. Also, with increasing temperature, the movement of polymer chain was maintained leading to the dipolar loss.

Overall, the charge carriers or dipoles at low frequencies can easily orient themselves with the electric field, which increase the mobility of polymer segments, leading to the high values of (ε′) and (ε″) observed at high temperatures [38]. But at high frequencies they cannot shift as fast as the applied field changes, resulting in the temperature independence of (ε′) and (ε″). Moreover, the enhancement observed in dielectric properties of PVVH/GO nanocomposites has stemmed from the possibility of forming microcapacitors structure due to the dielectric nature of PVVH that isolates GO sheets [15].

3.2.2 Electric modulus analysis

The dielectric moduli (M′ and M″) analysis is always used to reveal the real dipolar contribution owing to its effective role in suppressing the influence of electrode polarization [39]. Also, it provides a deeper insight into the charge transport mechanisms which can be useful in understanding electrical properties of the samples being investigated. The real part of electric modulus (M′) and the imaginary part (M″) can be written as follow [38]:

$$M' = \frac{\varepsilon'}{\varepsilon'^2 + \varepsilon''^2} \tag{4}$$

$$M'' = \frac{\varepsilon''}{\varepsilon'^2 + \varepsilon''^2} \tag{5}$$

The variation of (M′) of the prepared samples (PG0 and PG6, as examples) with temperature and frequency is shown in Fig. 7a, b, where the spectra are characterized by a part

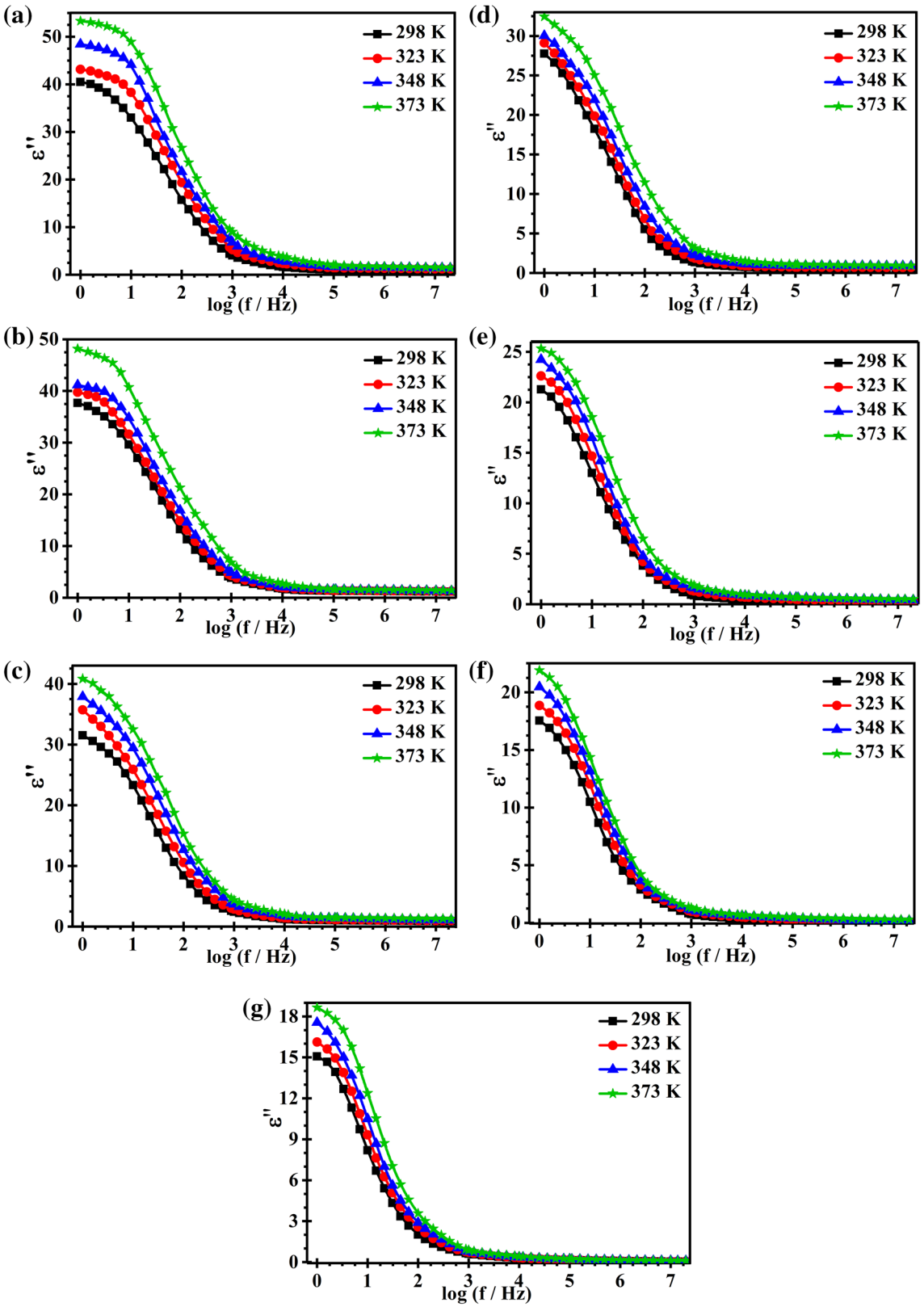

Fig. 6 The variation of (ε″) with frequency for **a** PG0, **b** PG1, **c** PG2, **d** PG3, **e** PG4, **f** PG5, **g** PG6 at various temperatures

of a sigmoid shape. It is observed that the value of (M′) at low frequencies approaches zero and the width of this part increased with the increase GO percentage within PVVH matrix as demonstrated in Fig. 7c, which indicates the successful suppression of electrode polarization effect [39]. Further, it exhibits a step-like transition with increasing frequency and then attains a constant value, implying that the current nanocomposite has a significant capacitive nature.

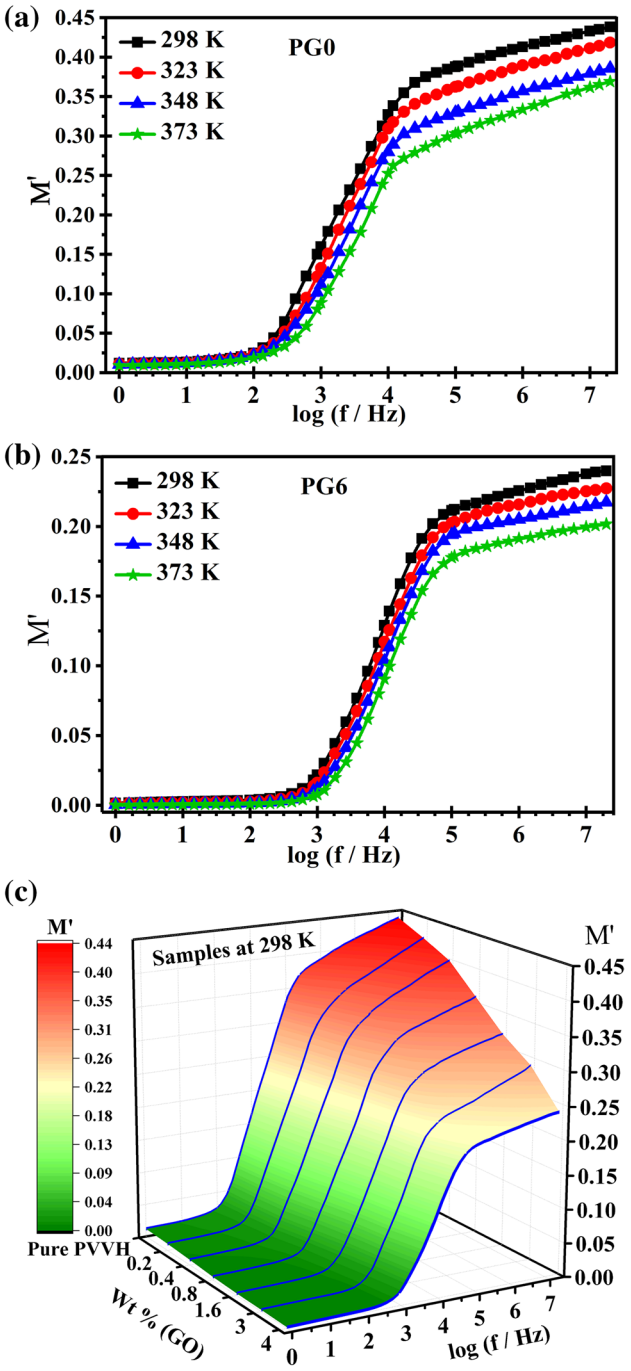

Fig. 7 The variation of (M′) for **a** PG0 and **b** PG6 (as examples) with temperature and frequency. **c** The frequency dependence of (M′) for the nanocomposites at different levels of GO recorded at room temperature

Figure 8a, b depicts the variation of (M″) with temperature and frequency, where the spectra are characterized by a well-defined dielectric relaxation peak. This loss peak is centered at a frequency [known as relaxation frequency (f_{max})] at which the step-like transition and dispersion took place as exhibited in (M′) spectra. Moreover, it is considered as a turning point from long-range motion of charge carriers [the low-frequencies side left to f_{max}] to short-range motion [the high-frequencies side right to (f_{max})]. Our experimental observation is in agreement with results reported by Amrin et al. [34]. It is also assigned to interfacial polarization effect, which represents the prevalent source of dielectric relaxation at PVVH–GO interfaces.

The charge carriers at lower frequencies can move freely, while at high frequencies, they undergo localized motion and are confined to a potential well [40]. It is noteworthy that, this distinct peak is shifted towards higher frequencies with increasing temperature, where more charge carriers are thermally generated, indicating that the conduction mechanism is hopping-type conduction.

Figure 8c shows the variation of (M″) for the nanocomposites with frequency at different levels of GO recorded at room temperature. The distinct decrease in (M″) with increasing GO loading provides a clear indication about the PVVH interaction with GO in the prepared nanocomposites. This decrease is in agreement with Maxwell–Wagner–Sillars (MWS) type of relaxation [38]. The difference between the conductive and dielectric nature of GO and PVVH, respectively has resulted in interfacial polarization, where the increase in GO content introduces new interfacial regions and increases the accumulation of free charge carriers in these regions. This accumulation reduced the relaxation time, consequently led to the shift observed in relaxation peak towards the higher frequencies, confirming the above observation.

In comparison with the symmetrical peak of the ideal Debye response, the observed broad peaks of PG0 and PVVH/GO nanocomposites are considered asymmetrical peaks.

The complex electric modulus (M*) can be written as follow [34, 38]:

$$M^* = M' + M'' = M_\infty \left[1 - \int_0^\infty \left\{\exp(-i\omega t)\left(\frac{-d\phi(t)}{dt}\right)\right\} dt\right] \quad (6)$$

where M_∞ is the asymptotic value and ϕ(t) is the Kohlrausch–Williams–Watts (KWW) function [41], defined by:

$$\phi(t) = \exp\left[-\left(\frac{t}{\tau_m}\right)^\beta\right] \quad (7)$$

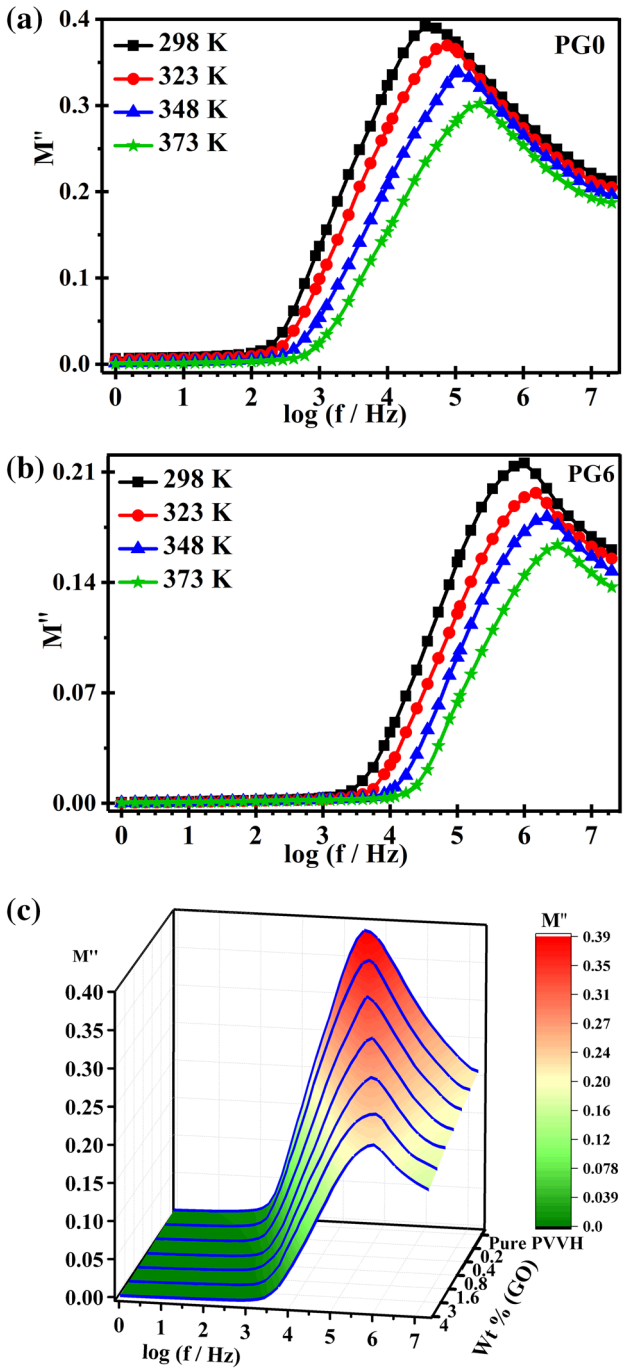

Fig. 8 The variation of (M″) for **a** PG0 and **b** PG6 (as examples) with temperature and frequency. **c** The variation of (M″) for the nanocomposites with frequency at different levels of GO recorded at room temperature

where τ_m is the conductivity relaxation time and β is a parameter linked to stretching with value $0<\beta\leq 1$. However, the single parameter [i.e., (β)], is not sufficient to elucidate the asymmetrical nature and broadness of (M″) spectra. So, in order to explain the asymmetrical nature of these peaks, a general equation for susceptibility should be assumed.

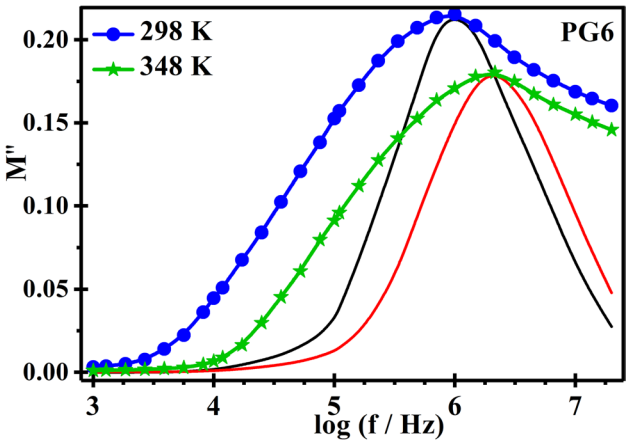

Fig. 9 Simulation of the ideal Debye response in comparison to the actual experimental results at 298 and 348 K for PG6 sample

According to Bergman equation [42] that depends on the modified KWW function, the relation between (M″) and its maximum value (M''_{max}) at (f_{max}) can be represented as:

$$M''(\omega)=\frac{M''_{max}}{\frac{1-c}{a+b}\left[b\left(\frac{f}{f_{max}}\right)^{-a}+a\left(\frac{f}{f_{max}}\right)^{b}\right]+c} \tag{8}$$

where a and b are independent parameters on shape for low and high frequencies, and c is a parameter related to smooth of the relaxation peak. For the ideal Debye response, $a=b=1$ and $c=0$, then Eq. (8) reduces to,

$$M''(\omega)=\frac{M''_{max}}{\frac{1}{2}\left[\left(\frac{f_{max}}{f}\right)+\left(\frac{f}{f_{max}}\right)\right]} \tag{9}$$

This equation, that represents simulation of the ideal Debye response, is shown in Fig. 9 in comparison to the actual experimental results at 298 and 348 K for PG6 sample. From this figure, it is revealed that the experimental data has deviated from the ideal Debye response, confirming the non-Debye behaviour of the samples.

3.2.3 Variation of loss tangent with frequency and temperature

Figure 10 shows the frequency dependence of loss tangent (tan δ) at 298 K of the studied samples at different levels of GO, where it has been calculated using the following equation,

$$\tan\delta=\frac{\varepsilon''}{\varepsilon'} \tag{10}$$

This figure is characterized by a broad peak observed in the dispersion region of the corresponding ε′. Further, this

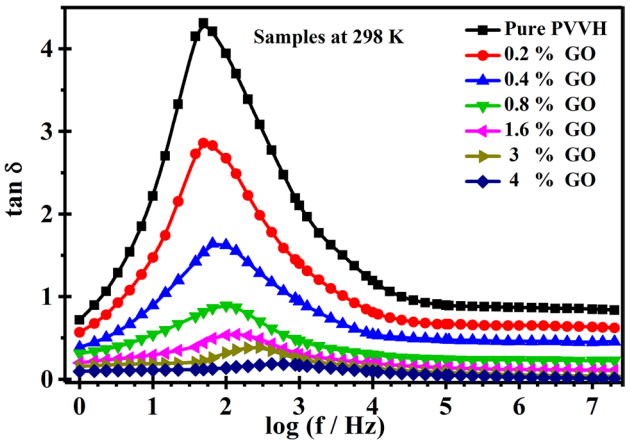

Fig. 10 The frequency dependence of loss tangent (tan δ) at 298 K of the studied samples at different levels of GO

peak is shifted towards higher frequencies with the increase in GO content, reducing the relaxation time due to accumulation of free charge carriers at the interfaces between PVVH and GO. The relaxation peak detected is assigned to β-relaxation [24], which is originated by orientation of the polar groups such as; OH, C–O and/or C=O in the current polymeric matrix. This type of relaxation is known as a dipolar group relaxation [43]. In other words, this broad peak is ascribed to the localized movements of the polymeric segments [44]. Moreover, the amorphous regions are characterized by the irregular and entangled chains, which make them more flexible, increasing their capability to orient themselves, whereas the chains in crystalline regions are regularly arranged. This irregularity leads to weakness in molecular packing and density of the amorphous regions which pave the way for enhancing conductivity.

The dipoles of C–O and O–H groups on the edges of the basal plane of GO will orient themselves at a certain frequency governed by two main forces, where the elastic restoring force, which keeps the dipoles at their equilibrium positions, is sufficient to push against the rotational frictional forces exerted by their neighbors [34, 45]. The rich of amorphous regions inside the PVVH/GO nanocomposites is useful for the dipolar molecules to orient themselves and absorbing energy over a wide range of frequency and temperature [39].

The relaxation times (τ) for the studied samples have been calculated using the formula $2\pi f_{max}\,\tau = 1$, and their values are presented in Table 1. From this table, it is found that their values are on the order 10^{-4} s suggesting that dipoles behavior in the applied electric field match well with Cole–Cole model [46], which confirms the results of dielectric constant. The decrease in relaxation time with the increase in temperature and GO loading into PVVH matrix is attributed to the increase in the movement of polymer chains and mobility of

Table 1 The activation energy (E_a) and relaxation time (τ) calculated for the PVVH-based nanocomposites

Samples	Activation energy (eV)	Relaxation time (s)
PG0	1.23	20.05×10^{-4}
PG1	1.11	14.90×10^{-4}
PG2	1.03	13.19×10^{-4}
PG3	0.95	11.50×10^{-4}
PG4	0.88	9.41×10^{-4}
PG5	0.8	5.00×10^{-4}
PG6	0.76	2.91×10^{-4}

charge carriers in the polymer matrix. This is also assigned to the reduction of free volume with increasing GO concentration. For example, the τ value for PG0 at room temperature is 20.04×10^{-4} s, whereas that of PG6 is 2.9×10^{-4} s. The later became 8.75×10^{-5} s at 373 K as shown in Fig. 11, which indicates thermally activated relaxation for the charge carriers. The same behaviour has been reported by Chen et al. [34, 38, 47].

Figure 11 exhibits the frequency–temperature dependence of (tan δ) for PG6 sample, where its value is found to be tan δ = 0.19 at room temperature and decreased to 0.13 at 373 K. Rathod et al. [48] reported that the best value of tan δ was 10 for PVA/GO composite at 5 wt% of GO at room temperature, while Chakraborty et al. [49] found that its value was 350 for 10 wt% of MWCNT incorporated into PVA at 423 K. This gives our nanocomposites in the current work a comparative advantage over other composites by using only 4 wt% of GO. The activation energy associated with relaxation process (E_a) was determined by plotting $\log f_{max}$ versus reciprocal of temperature as in Fig. 11 (inset) according to the following relation [12, 50],

$$f_{max} = f_o e^{-E_a/KT} \tag{11}$$

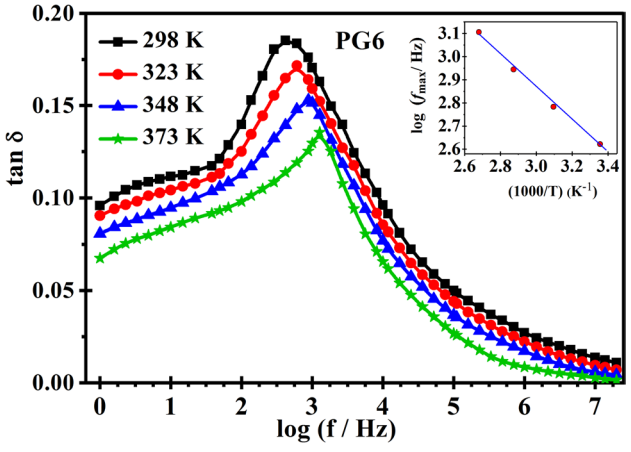

Fig. 11 The frequency–temperature dependence of (tan δ) for PG6 sample

The (E_a) values are listed in Table 1. It is evident that (E_a) values decreased with the increase in GO loading into PVVH matrix. This amount of energy is ascribed to the quantum confinement, where it is used for charge carriers to overcome the potential barrier that restrict them during relaxation process. This decrease indicated that the potential wells in PVVH/GO nanocomposites became less deep than that of the pure copolymer due to the addition of GO. Finally, it is observed that (tan δ) became relatively constant at high frequencies, which suggest the feasibility of using these nanocomposites in high frequency devices.

3.3 AC conductivity analysis

AC conductivity (σ_{ac}) has been calculated due to its effective role in understanding charge carriers transport mechanism and in clarifying how does incorporation of GO affects the electrical properties of the PVVH/GO nanocomposites. The frequency dependence of (σ_{ac}) for the prepared samples was investigated under various isothermal stabilization in the temperature range 298–373 K. Results obtained for PG0 and PG6 samples are shown in Fig. 12a, b as examples. The enhancement of (σ_{ac}) with increasing frequency and temperature indicates the presence of charge carriers transported via hopping through defect sites along the polymer chain [51].

Furthermore, it was increased with the increment in percentage of GO inside PVVH matrix at 298 K as demonstrated in Fig. 13. The conductivity has a frequency-independent behaviour in the low frequency region, where its value increases at a very small rate, approaching its DC value. On the contrary, a frequency dependent behavior has appeared in the higher-frequency region, where its value increased rapidly with frequency. In other words, charge carriers move over long-range distances by applying electric field with low frequency, while with increasing the applied frequency, their relative movements are changed to short-range distances, where conductivity exponentially increases with frequency. The measured conductivity σ (ω) can be expressed as [52]:

$$\sigma(\omega) = \sigma_{dc} + C\omega^{S} \quad (12)$$

where, σ_{dc} is the DC conductivity of the sample under investigation and it is considered as the frequency independent part, C is a temperature dependent constant, ω is an angular frequency given by $\omega = 2\pi f$, S is a frequency dependent exponent ($0 < S < 1$), and $\sigma_{ac} = C\omega^{S}$ is the real part that represents AC conductivity and follows Jonscher's universal power law that characterizes the amorphous materials [53].

The enhancement in (σ_{ac}) at high frequencies is attributed to the increase in the number of free charge carriers that were trapped and confined to potential wells. In addition to the formation of conductive network via some sheets of GO which were not covered completely by PVVH. This helped charge

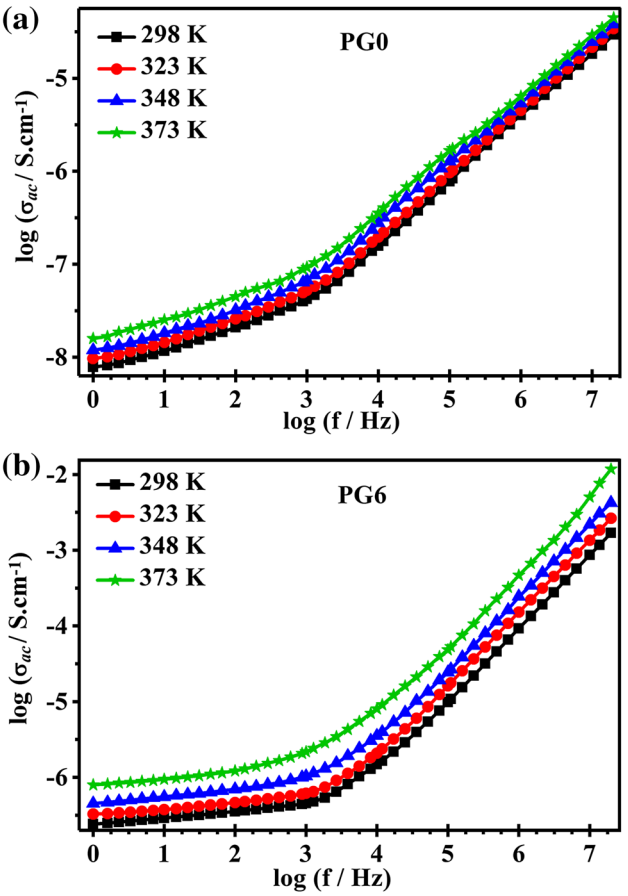

Fig. 12 The frequency dependence of (σ_{ac}) for **a** PG0 and **b** PG6 samples in the temperature range 298–373 K

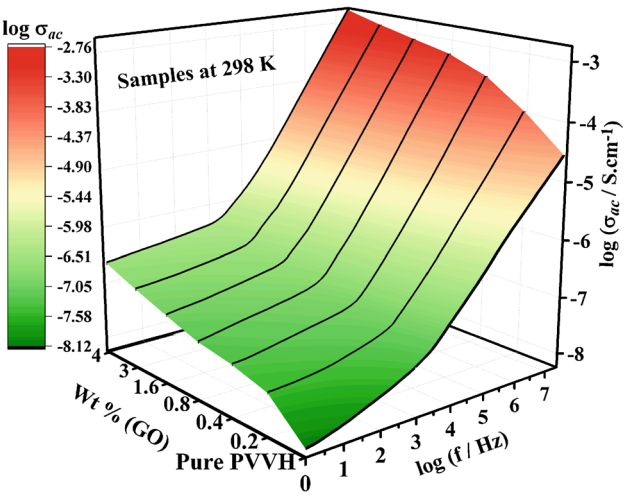

Fig. 13 The frequency dependence of (σ_{ac}) at 298 K of the studied samples at different levels of GO

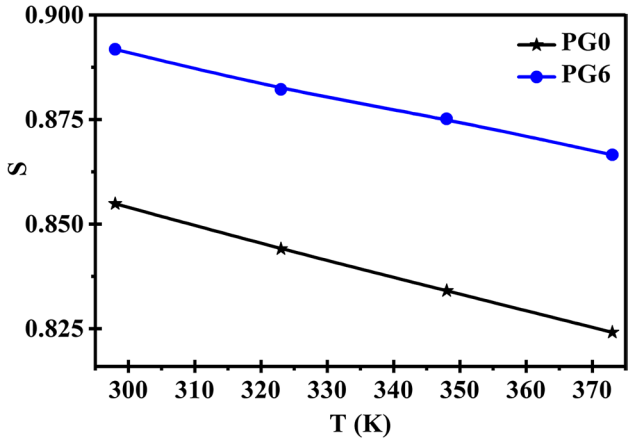

Fig. 14 The variation of exponent (S) with temperature for PG0 and PG6 samples as examples

carriers to move from one site to another within the PVVH matrix, resulting in the observed increase in conductivity.

By plotting log (σ_{ac}) versus log (f) at different temperatures, the exponent (S) values were calculated using slopes of the curves resulted and are displayed in Fig. 14 for PG0 and PG6 samples as examples.

In an attempt to describe the temperature–frequency dependence of (σ_{ac}) and its relation with the (S) values, many theoretical models have been buildup for AC conductivity in amorphous materials. The models depended on relaxation that resulted from passing of charge carriers by tunneling or hopping through defect sites over the potential barriers separating them [54, 55].

In details, these models can be compared by distinguishing their relation to temperature as follows: the frequency exponent is independent on temperature (T) in the quantum mechanical tunneling model (QMT), while in the small-polaron tunneling model (SPT), it increases with increasing (T). But the correlated barrier hopping model (CBH) is dominant when (S) decreases with the increase in (T) and in case of the overlapping large-polaron model (OLP), (S) also decreases with (T) reaching a minimum value then followed by an increase in its value [54]. So, the decrease in (S) values with increasing (T) is shown in Fig. 14, which indicates that CBH is the predominant conduction mechanism inside the prepared samples. In other words, CBH model is the best choice among the previously mentioned models for describing AC conduction mechanism in the current nanocomposites, and the relation between (S) and (T) can be written as follow [34, 56]:

$$S = 1 - \frac{6KT}{W_m - KTln\left(\frac{1}{\omega\tau_m}\right)} \tag{13}$$

where K is Boltzmann's constant and W_m is the maximum barrier height. For small temperature, $W_m \gg KT \ln\left(\frac{1}{\omega\tau_m}\right)$ and Eq. (12) reduces to [57]:

$$S = 1 - \frac{6KT}{W_m} \tag{14}$$

The maximum barrier height can be calculated via substituting by (S) and (T) values in Eq. (14) and the results obtained are listed in Table 2. The observed decrease in (W_m) with increasing temperature is ascribed to the increase in amorphous regions inside the prepared samples. The same behaviour was reported by Aziz et al. and El-Mallah [58, 59]. It is noteworthy that W_m value is lower than (E_a), confirming that conduction mechanism within the current nanocomposites takes place by hopping transport [59], which proves that CBH model was the correct choice for describing the AC conduction mechanism.

3.4 Scaling of AC conductivity

To get a deeper insight into AC conduction in the current system, we used scaling of conductivity owing to its ability to collapse the spectra obtained to a single master curve which clarifies the common conduction mechanism within the prepared samples.

According to Summerfield method, the scaling of AC conductivity can be represented via the following relation [26, 60]:

$$\frac{\sigma}{\sigma_{dc}} = F\left(\frac{f}{\sigma_{dc}T}\right) \tag{15}$$

It is evident from Fig. 15 that the σ_{ac} spectra of the current nanocomposites at different levels of GO largely overlaps into a single master curve, signifying that the charge carriers within the current samples follow a common conduction mechanism and are independent on the dopant concentration [61].

3.5 Morphological study

The morphology and interfacial adhesion of PVVH/GO nanocomposites with varying levels of GO have been investigated by employing scanning electron microscopy (SEM).

Table 2 The maximum barrier height (W_m) for PG0 and PG6 samples

Temperature(K)	W_m (eV)	
	PG0	PG6
298	0.942	0.712
323	0.934	0.700
348	0.922	0.668
373	0.912	0.648

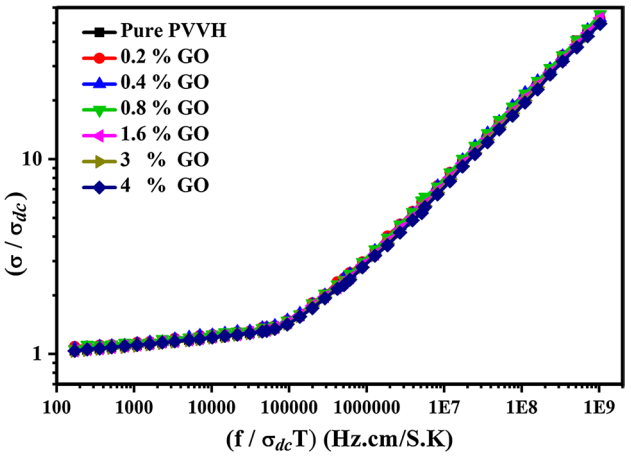

Fig. 15 Scaling of AC conductivity of the studied samples with varying concentration of GO

The SEM microstructure of the prepared samples (PG0 and PG6 as examples) is depicted in Fig. 16. It evident that the surface of PG0 was relatively smooth, but its sate changed to rough as GO was added (PG6). This increase in roughness is a good indication about the compatibility between PVVH and GO where no phase separation was observed. Moreover, it confirms the well-interfacial adhesion between the polymer and the filler which is highly desirable to improve the nanocomposite performance.

3.6 Mechanical properties

Figure 17 exhibits stress–strain curves of PG0 and the PVVH/GO nanocomposites. Incorporation of GO into PVVH matrix has significantly enhanced both tensile strength and Young's modulus, while elongation at break has decreased relatively compared to that of pure PVVH. The forth mentioned parameters were calculated and listed in Table 3.

This improvement has been attained by addition of only 4 wt% of GO to the polymer matrix, giving our nanocomposites a comparative advantage over other composites [62–64]. The tensile strength has increased from 17.11 to 67.29 MPa, i.e., by 293.28%, in addition to the increase of Young's modulus from 1.14 to 8.97 MPa, i.e., by 686.8%. This is due to the strong interaction between GO and PVVH and the homogeneous dispersion of GO. However, the elongation at break has decreased from 65 to 12.5 i.e., by 80.8% for PG6 sample. This behaviour is in agreement with previous reports in literature [25, 65]. So, it's noteworthy that the significant enhancement in mechanical properties of the prepared nanocomposites is ascribed to the good interfacial adhesion of the polymer matrix with GO, where it largely limits the movement of PVVH chains.

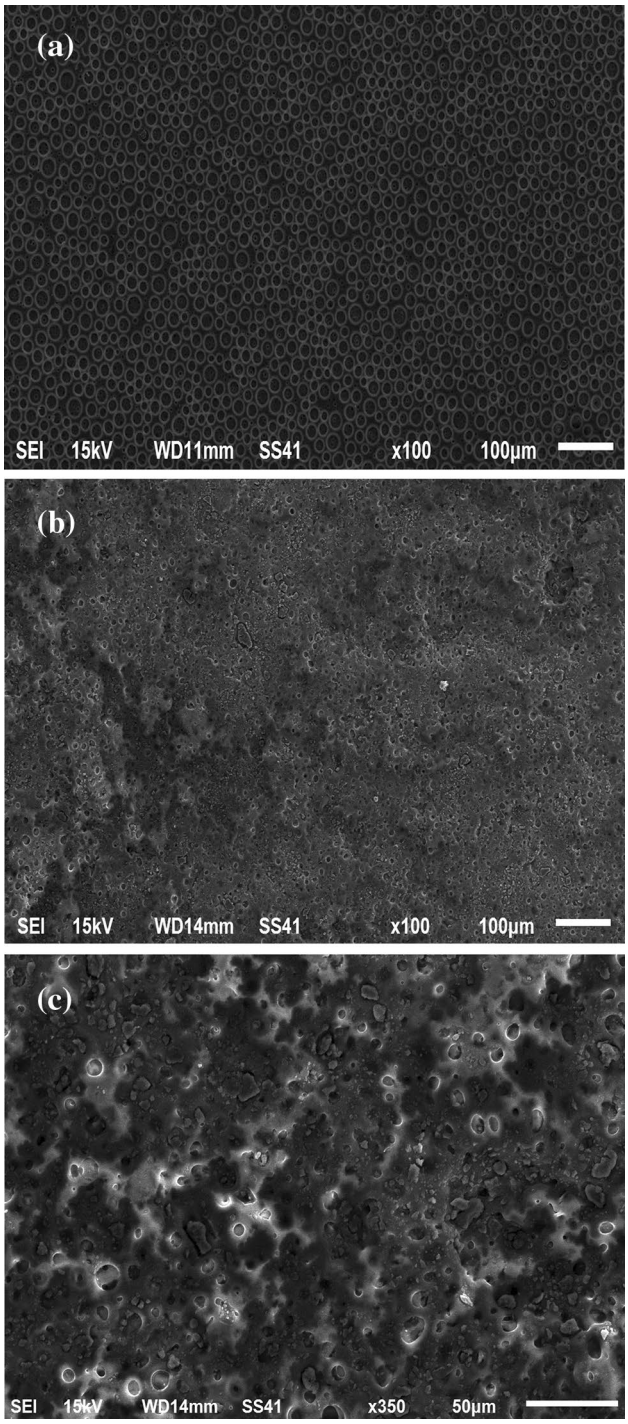

Fig. 16 The SEM micrographs of: **a** PG0 and **b** PG6 (as examples) at magnification 100 times and **c** PG6 at magnification 350 times

4 Conclusion

XRD, FT-IR and Raman studies showed that GO has been synthesized and efficiently exfoliated into individual sheets. PVVH-based nanocomposites have been successfully prepared via solution casting technique with varying

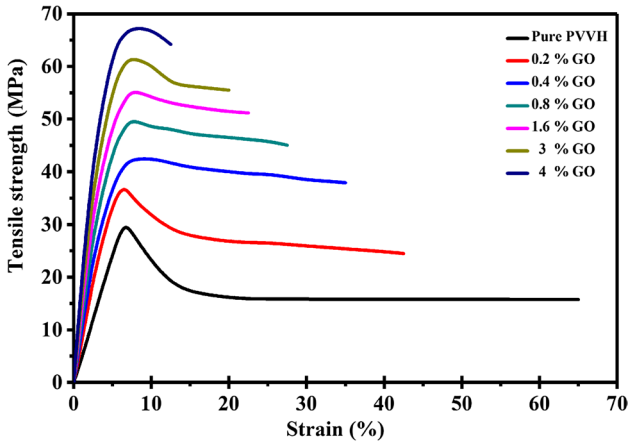

Fig. 17 Stress–strain curves of the studied samples at different levels of GO

Table 3 The tensile strength, Young's modulus and elongation at break for the prepared samples

Samples	Tensile strength	Young's modulus	Elongation at break (%)
PG0	17.11	1.14	65
PG1	37.55	5.78	42.5
PG2	42.40	6.06	35
PG3	50.13	6.68	27.5
PG4	55.69	7.43	22.5
PG5	61.73	8.23	20
PG6	67.29	8.97	12.5

GO loading in the PVVH matrix. The SEM results and the enhanced mechanical properties confirm the compatibility and the well-interfacial adhesion between GO and PVVH, which is highly desirable to improve the nanocomposite performance. The dielectric properties and AC conductivity of the prepared nanocomposites have been investigated. The improved dielectric constant of PVVH/GO nanocomposites with the increase in GO content and temperature is ascribed to the formation of microcapacitors within the polymer matrix. The electric modulus constant exhibited a step-like transition with the increase in frequency, implying that the current nanocomposite has a significant capacitive nature. The asymmetrical nature of (M″) spectra confirmed the non-Debye behaviour of the prepared nanocomposite. The AC conductivity and the maximum barrier height prove that the CBH model is the best choice for describing AC conduction mechanism where charge carriers transport via hopping through defect sites along the polymer chain. Thus, these findings promote PVVH/GO nanocomposites to be used for development of electrochemical and energy storage devices.

References

1. R. Raccichini, A. Varzi, S. Passerini, B. Scrosati, Nat. Mater. **14**, 271–279 (2015)
2. K.R. Nemade, S.A. Waghuley, J. Electron. Mater. **42**, 2857–2866 (2013)
3. C.G. Liu, Z.N. Yu, D. Neff, A. Zhamu, B.Z. Jang, Nano Lett. **10**, 4863–4868 (2010)
4. Q. Chi, T. Ma, Y. Zhang, Y. Cui, C. Zhang, J. Lin, X. Wang, Q. Lei, J. Mater Chem. A **5**, 16757–16766 (2017)
5. Z. Pan, B. Liu, J. Zhai, L. Yao, K. Yang, B. Shen, Nano Energy **40**, 587–595 (2017)
6. B.F. Machadoab, P. Serp, Catal. Sci. Technol. **2**, 54–75 (2012)
7. C. Bora, S.K. Dolui, Polym. **53**, 923–932 (2012)
8. A.K. Geim, K.S. Novoselov, Nat. Mater. **6**, 183–191 (2007)
9. P. Mukhopadhyay, R.K. Gupta, *Graphite, Graphene, and their Polymer Nanocomposites* (CRC Press, Taylor & Francis Group, Boca Raton, 2013)
10. J. Guan, C. Xing, Y. Wang, Y. Li, J. Li, Compos. Sci. Technol. **138**, 98–105 (2017)
11. I. Latif, T.B. Alwan, A.H. Al-Dujaili, Nanaosci. Nanaotechnol. **2**, 190–200 (2012)
12. I. Tantis, G.C. Psarras, D. Tasis, Express Polym. Lett. **6**, 283–292 (2012)
13. Z. Pan, L. Yao, J. Zhai, X. Yao, H. Chen, Adv. Mater. **30**, 1705662–1705668 (2018)
14. J. Chen, X. Yu, F. Yang, Y. Fan, Y. Jiang, Y. Zhou, Z. Duan, J. Mater. Sci. **28**, 8043–8050 (2017)
15. Z. Wang, R. Wei, X. Liu, J. Electron. Mater. **46**, 488–496 (2017)
16. Y.-C. Cao, C. Xu, X. Wu, X. Wang, L. Xing, K. Scott, J. Power Sources **196**, 8377–8382 (2011)
17. P. Chammingkwan, K. Matsushita, T. Taniike, M. Terano, Mater. **9**, 240–253 (2016)
18. S.S. Tzeng, F.Y. Chang, Mater. Sci. Eng. A **302**, 258–267 (2001)
19. Z. Lei, Y. Jun-He, W. Xian-Ying, H. Xing, Z. Bin, T. Zhi-Hong, Y. Guang-Zhi, Q. Han-Xun, Chin. Phys. Lett. **28**, 016501–016503 (2011)
20. A.M. Abdelghany, M.A. Morsi, A. Abdelrazek, M.T. Ahmed, Silicon **10**, 519–524 (2018)
21. M. Migahed, M. Ahmed, Polym. Plast. Technol. Eng. **43**, 1053–1066 (2004)
22. M. Ahmed, T. Fahmy, Polym. Plast. Technol. Eng. **44**, 1559–1572 (2005)
23. M. Ahmed, T. Fahmy, J. Korean Phys. Soc. **59**, 98–104 (2011)
24. K. Deshmukh, M.B. Ahamed, K.K. Sadasivuni, D. Ponnamma, M.A. AlMaadeed, S.K.K. Pasha, R.R. Deshmukh, K. Chidambaram, Mater. Chem. Phys. **186**, 188–201 (2017)
25. S.W. Kim, H.M. Choi, High Perform. Polym. **27**, 694–704 (2015)
26. M. Devi, A. Kumar, Mater. Res. Bull. **97**, 207–214 (2018)
27. X. Zhao, Q. Zhang, Y. Hao, Y. Li, Y. Fang, D. Chen, Macromol. **43**, 9411–9416 (2010)
28. W.S. Hummers, R.E. Offeman, J. Am. Chem. Soc. **80**, 1339 (1958)
29. J. Yan, Y. Huang, C. Wei, N. Zhang, P. Liu, Composites Part A **99**, 121–128 (2017)
30. V. Kavimani, S. Prakash, K. Rajesh, R.D. Rammasamy, N.B. Selvaraj, T. Yang, B. Prabakaran, S. Jothi, Appl. Surf. Sci. **424**, 63–71 (2017)
31. S. Frindy, A. Primo, H. Ennajih, A. Qaiss, R. Bouhfid, M. Lahcini, E. Essassi, H. Garcia, A. El Kadib, Carbohydr. Polym. **167**, 297–305 (2017)
32. P. Hedvig, *Dielectric Spectroscopy of Polymer* (Adam Hilger, Bristol, 1977)
33. G. Gondivaraj, N. Baskaran, K. Shahi, P. Monoravi, Solid State Ionics **76**, 47–55 (1995)
34. S. Amrin, V.D. Deshpande, Physica E **87**, 317–326 (2017)

35. M. Hema, S. Selvasekerapandian, A. Sakunthala, D. Arunkumar, H. Nithya, Physica B **403**, 2740–2747 (2008)
36. A.Y. Yassin, *Spectroscopic and Physical Studies of Some Polymers Doped with Metallic Halides* (M.Sc. Thesis, Mansoura University, Mansoura, 2010)
37. S.P. Mondal, R. Aluguri, S.K. Ray, J. Appl. Phys. **105**, 114317–114323 (2009)
38. S. Sinha, S.K. Chatterjee, J. Ghosh, A.K. Meikap, J. Mater. Sci. **50**, 1632–1645 (2015)
39. C.V.S. Reddy, X. Han, Q.Y. Zhu, L.Q. Mai, W. Chen, Microelectron. Eng. **83**, 281–285 (2006)
40. J.S. Kim, J. Phys. Soc. Jpn. **70**, 3129–3133 (2001)
41. G. Williams, D.C. Watts, Trans. Faraday Soc. **66**, 80–85 (1970)
42. R. Bergman, J. Appl. Phys. **88**, 1356–1365 (2000)
43. K. Pandey, M.M. Dwivedi, M. Singh, S.L. Agrawal, J. Polym. Res. **17**, 127–133 (2010)
44. E. Suljovrujic, M. Micic, D. Milicevic, J. Eng. Fiber Fabr. **8**, 131–143 (2013)
45. V. Raja, A.K. Sharma, V.V.R.N. Rao, Mater. Lett. **58**, 3242–3247 (2004)
46. R. Dutta, A. Kumar, J. Phys. D **50**, 425302–425312 (2017)
47. T. Chen, B. Liu, Mater. Lett. **209**, 163–166 (2017)
48. S.G. Rathod, R.F. Bhajantri, V. Ravindrachary, P.K. Pujari, T. Sheela, J. Naik, AIP Conf. Proc. **1591**, 1769–1771 (2014)
49. G. Chakraborty, A.K. Meikap, R. Babu, W.J. Blau, Solid State Commun. **151**, 754–758 (2011)
50. P.B. Bhargav, V.M. Mohan, A.K. Sharma, V.V.R.N. Rao, Curr. Appl. Phys. **9**, 165–171 (2009)
51. S. Saravanan, M. Anantharaman, S. Venkatachalam, Mater. Sci. Eng. B **135**, 113–119 (2006)
52. S. Banerjee, A. Kumar, J. Appl. Phys. **109**, 114313–114321 (2011)
53. A.K. Jonscher, Nature **267**, 673–679 (1977)
54. S. Ebrahim, A.-H. Kashyout, M. Soliman, Curr. Appl. Phys. **9**, 448–454 (2009)
55. N. Mott, E. Davis, *Electronic Processes in Non-crystalline Materials* (Oxford University Press, New York, 1979)
56. P. Dutta, S. Biskas, M. Ghosh, S. De, S. Chatterjee, Synth. Met. **122**, 455–461 (2001)
57. K. Hayat, M.A. Rafiq, S.K. Durrani, M.M. Hasan, Physica B **406**, 309–314 (2011)
58. S.B. Aziz, R.M. Abdullah, M.A. Rasheed, H.M. Ahmed, Polymers **9**, 338–356 (2017)
59. H.M. El-Mallah, Acta Phys. Pol. A **122**, 174–179 (2012)
60. S. Summerfield, Philos. Mag. B **52**, 9–22 (1985)
61. J. Hazarika, A. Kumar, Synth. Met. **198**, 239–247 (2014)
62. D. Ponnamma, K.K. Sadasivuni, M. Strankowski, P. Moldenaers, S. Thomas, Y. Grohens, RSC Adv. **3**, 16068–16079 (2013)
63. W.K. Zhu, H.P. Cong, H.B. Yao, L.B. Mao, A.M. Asiri, K.A. Alamry, H.M. Marwani, S.H. Yu, Small **11**, 4298–4302 (2015)
64. Y. Jin, G. Huang, D. Han, P. Song, W. Tang, J. Bao, R. Li, Y. Liu, Composites Part A **86**, 9–18 (2016)
65. M. Tayebi, A. Ramazani S.A., M.T.H. Mosavian, A. Tayyebi, Polym. Adv. Technol. **26**, 1083–1090 (2015)